



Commissioning of a Coherent Radiation THz Spectrometer for Electron Beam Diagnostics at FLASH2

Tanish Satoor, University of Cambridge, UK

October 4, 2017

Abstract

The Free Electron Laser in Hamburg (FLASH) accelerates bunches of electrons which have been compressed to typical lengths of 10 fs. Diagnostic tools measuring the bunches' longitudinal structure are required for precise compression control. A THz spectrometer was commissioned at FLASH2 to achieve this. The instrument is designed to measure broadband coherent diffraction or transition radiation spectra from compressed electron bunches. The beamline from FLASH2 to the spectrometer was calibrated and aligned firstly using an optical laser and then with the diffraction radiation itself. This alignment was also carried out for the spectrometer's internal optics. Functionality checks were carried out on all components and known problems were fixed. Initial spectra measurements strongly indicate that the commissioning was successful, but some further checks and fixes are needed before it can be used for diagnostics.

Contents

1	Introduction	3
2	Theoretical Background	5
2.1	Coherent Radiation Spectroscopy	5
2.2	Linear Ray Optics	5
3	Technical Commissioning	7
3.1	THz Beamline	7
3.1.1	Alignment and Calibration Procedure	7
3.1.2	Results and Discussion	9
3.1.3	Calibration Check	11
3.2	THz Spectrometer	13
3.2.1	Functionality Checks and Alignment	13
4	Beam Based Commissioning	15
4.1	Measuring Intensity	15
4.2	THz Beamline Re-Alignment	15
4.3	Internal Spectrometer Alignment	17
5	First Measurements of Spectra	21
5.1	Methods	21
5.2	Results and Discussion	23
6	Conclusions	25

1 Introduction

The Free Electron Laser in Hamburg (FLASH) accelerates bunches of electrons which then pass through alternating magnetic fields to generate bright, soft X-ray pulses[1, 2]. The radiation produced is used for a wide range of experiments in life science, chemistry and physics. The electron bunches required to drive the Self Amplified Stimulated Emission (SASE) process generating this radiation must have high peak currents in the kA range and hence are compressed from 1 ps (RMS) to typical lengths of 10 fs. The longitudinal profiles of these bunches must be measured for diagnostics, enabling precise compression control.

FLASH1 currently has a THz spectrometer and a microwave transverse deflecting structure (TDS)[3, 7] for longitudinal diagnostics. However, FLASH2 currently lacks such a device. The aim of this project was the commissioning of a coherent radiation THz spectrometer for this purpose.

The spectrometer is positioned after the linear accelerator section in the FLASH2 tunnel and before the undulators (See Figure 1). At the spectrometer station, compressed ultra-relativistic electron bunches pass through an aperture in metallic screen, and emit radiation due to the change in dielectric constant in the vicinity of their trajectory. This radiation is transported out of the electron beamline by a THz beamline to the spectrometer. As seen in Figure 2, the spectrometer consists of four gratings which disperse progressively longer wavelengths. The dispersed radiation is reflected onto detector arrays where its intensity is measured using broadband pyroelectric detectors connected to fast readout electronics. The gratings can be remotely switched between two sets, allowing for spectral measurements in the 5 μm to 435 μm wavelength range.

As described in the next section, measurement of the spectra of the coherent radiation emitted enables reconstruction of the structure of the bunch. In this way, the spectrometer can be used as a longitudinal bunch diagnostics tool. Similar spectrometers have successfully been used to reconstruct bunch profiles in the past [10, 11].

Section 3 describes the technical commissioning of the spectrometer, including functionality checks of all components and the initial alignment of the set-up using an optical laser. Section 4 describes the beam based commissioning, including the final alignment of the THz beamline and the spectrometer incoupling mirrors using the actual coherent diffraction radiation (CDR). It goes on to present the first spectra measured by the instrument. Section 6 summarises the work done and discusses the future outlook.

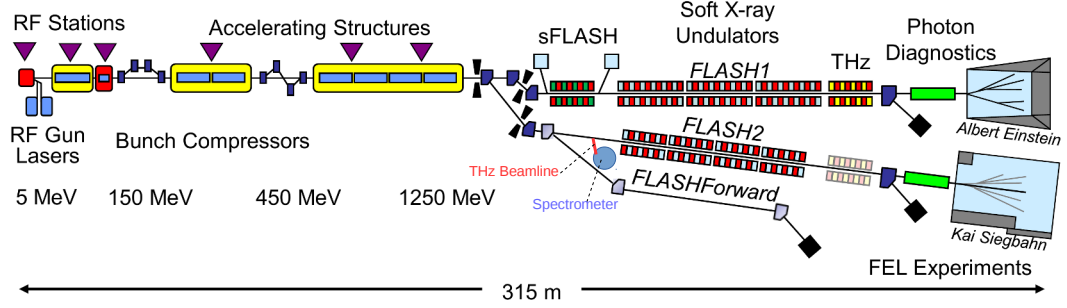


Figure 1: Schematic layout of FLASH. Our set-up is located at 182m within the FLASH2 tunnel. It is between the linac and undulator sections. The THz beamline (red) transports the coherent diffraction or transition radiation produced by electron bunches to the spectrometer (blue) for measurement.

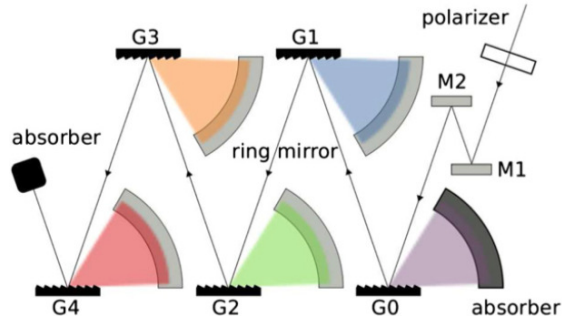


Figure 2: Layout of the spectrometer. A sequence of gratings with progressively wider spacings disperses short wavelengths to a detector array via a ring mirror. Longer wavelengths are reflected further along the marked optical path. The gratings can be replaced by another set remotely allowing for intensity measurements in the wavelength range $5\mu\text{m}$ to $435\mu\text{m}$ in 240 channels.

2 Theoretical Background

2.1 Coherent Radiation Spectroscopy

Broadband electromagnetic radiation is produced when a single relativistic electron is incident on or passes near a metallic screen. This is called transition radiation (TR) or diffraction radiation (DR) respectively. One possible interpretation explaining this phenomena is that the radiation results from an annihilation of the electron and its mirror charge upon arrival at the screen. The radiation's spectrum and distribution can be calculated analytically for screens with symmetric geometries e.g. an infinite plane, or a circular screen with a circular aperture in the centre[4].

Now consider a bunch containing N electrons, with a longitudinal particle density $\rho(z)$ and a characteristic length L . For wavelengths $\lambda \ll L$ the electrons act as independent incoherent sources and the intensity emitted scales as N . However, if λ is comparable to L the radiation from each electron interferes coherently and the intensity scales as N^2 . In fact, the longitudinal structure of the bunch in Fourier space is imprinted in the intensity spectrum through the relation:

$$\frac{dU}{d\lambda} = \left(\frac{dU}{d\lambda}\right)_1 \cdot (N + N(N-1) |F(\lambda)|^2). \quad (1)$$

where $\left(\frac{dU}{d\lambda}\right)_1$ is the spectrum emitted by a single electron and $F(\lambda)$ is the longitudinal form factor given by:

$$F(\lambda) = \int_{-\infty}^{\infty} \rho(z) e^{-2\pi i z / \lambda} dz. \quad (2)$$

Hence measuring the spectrum gives $|F(\lambda)|$, after which reconstruction techniques can be used to recover its phase and ultimately reconstruct $\rho(z)$. $|F|$ is in the range 0 to 1, which limits coherent spectral intensity. Figure 3 shows theoretical form factors for electron bunches with Gaussian density profiles.

For typical bunches at FLASH, $N \sim 10^{11}$ and hence the second, coherent term in Equation (1) dominates. The bunch lengths are typically 10 fs, and hence the spectrometer operates in the THz frequency regime. See [5, 6] for a detailed treatment of TR, DR, and the reconstruction procedure.

2.2 Linear Ray Optics

The linear ray transfer matrix formalism described here is used during optical alignment procedures further in the project. Working in one dimension for clarity, a light beam (eg. from an optical alignment laser) is a ray, described at any point along the set-up by a column vector $[x, x']$. Here, x and x' are the linear offset and angular deflection respectively from the optical axis.

We expect propagation by a distance s to change the ray vector to $[x + x' \cdot s, x']$, which can be represented as a multiplication by a propagation matrix

$$S = \begin{bmatrix} 1 & s \\ 0 & 1 \end{bmatrix}.$$

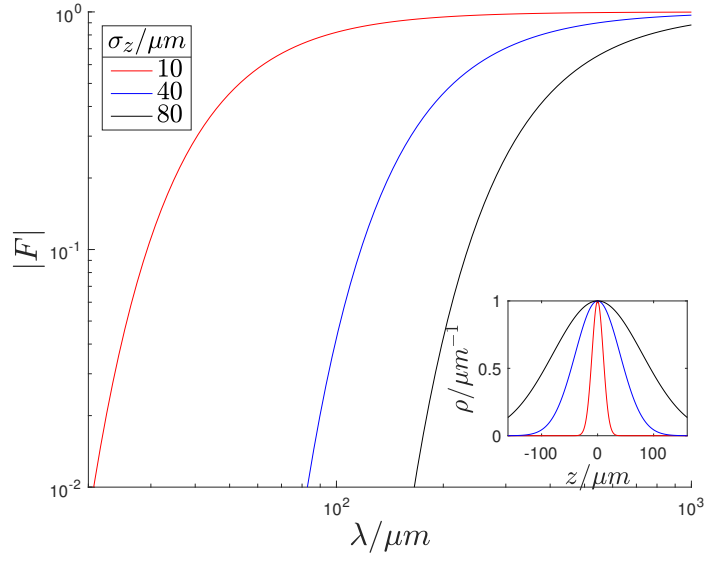


Figure 3: Analytic form factors for Gaussian bunches with different RMS lengths. The inset shows the respective longitudinal bunch profiles. A Gaussian bunch with RMS length σ_z has a profile $\rho(z) = \exp[-(z/\sigma_z)^2/2]$ and hence by Fourier transformation a form factor $F(\lambda) = \exp[-2(\pi \cdot \sigma_z/\lambda)^2]$. Shorter bunches have a greater form factor and hence a higher TR/DR spectral intensity at short wavelengths. Both axes are scaled logarithmically.

Similarly, reflection from a converging mirror of focal length $f(> 0)$ is described by the matrix

$$M = \begin{bmatrix} 1 & 0 \\ -\frac{1}{f} & 1 \end{bmatrix}.$$

Finally, a tilt in the mirror with respect to the optical axis may cause an additional angular deflection represented as addition of a ‘kick’ vector $[0, k]$. Hence an optical set-up with multiple elements like the THz beamline described in the next section can be treated using successive matrix multiplications and kick additions. This allows us to calculate the required tilts at each mirror to achieve a given final beam configuration.

3 Technical Commissioning

The technical commissioning is the first stage of the project. It includes the initial alignment of the THz beamline and spectrometer optics, in addition to functionality checks of all components. It was carried out during the FLASH2 shutdown i.e. when physical access to the spectrometer area located within the FLASH2 tunnel is possible.

3.1 THz Beamline

The THz beamline transports coherent radiation emitted by electron bunches at the radiation screen on the axis of the FLASH2 electron beam to the spectrometer vessel located inside the tunnel. The layout of the beamline is outlined in Table 1. This work used a $35\text{ mm} \times 30\text{ mm}$ DR screen with a $20\text{ mm} \times 10\text{ mm}$ rectangular aperture at its centre. The FLASH electrons pass through the aperture and produce DR, allowing for simultaneous user operation and diagnostics.

The screen is oriented at 45° to the electron beam axis. Hence, the coherent DR produced in the backward sphere is coupled out through the diamond window to the first section of the beamline which is perpendicular to FLASH. The next elements are four converging toroidal mirrors. Each mirror is attached to two remotely controllable stepper motors which can tilt it in two perpendicular directions. Each mirror is oriented at 45° to the optical axis and hence deflects the beam by 90° . The 2.7 m long beamline ends at a flange where the spectrometer was attached to it after initial alignment. The entire beamline and the spectrometer are maintained at below $1 \cdot 10^{-3}$ mbar to minimise atmospheric absorption. The beamline is based on previous ones described in further detail in [4] and [9].

3.1.1 Alignment and Calibration Procedure

An optical alignment laser ($\lambda = 637\text{ nm}$) was coupled to the beamline through a window at the screen chamber directly opposite to the diamond window (See Figure 4 (a)). The laser beam follows the same path as coherent radiation produced at the screen. The beamline was built up one segment at a time. An initial rough alignment was carried out by adjusting the motors such that the beam is centred on the mirrors and thus at the flanges connecting different segments. A flange cap with a marked central point was

Element	Absolute position (mm)	Focal length (mm)
Radiation Screen (on beam axis)	0	-
Diamond Window	70	-
Mirror 1	383	410
Mirror 2	623	980
Mirror 3	1015	980
Mirror 4	2075	840
End Flange (spectrometer entrance)	2718.4	-

Table 1: Layout of the THz beamline used to transport coherent radiation produced by electrons at the screen to the spectrometer vessel. Each toroidal converging mirror is oriented to deflect the beam by 90°

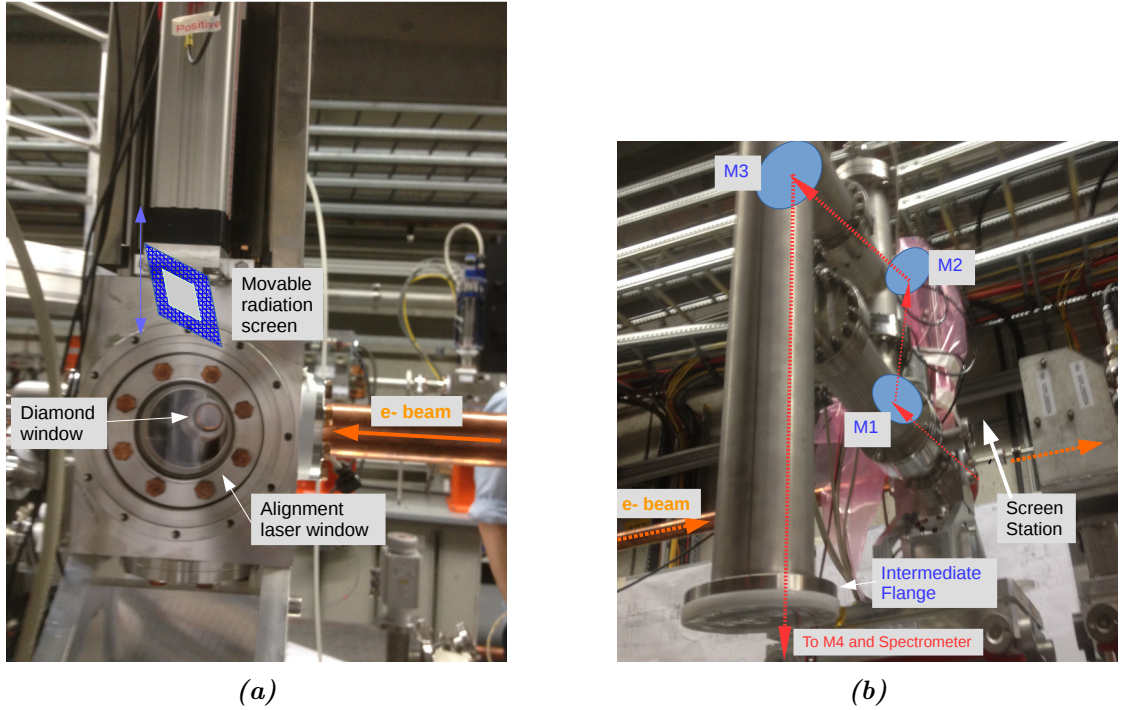


Figure 4: The THz beamline. (a) shows the screen station as viewed from directly opposite the start of the beamline. The window onto which an optical laser was flanged for alignment purposes is visible. The diamond window which separates the vacuum of the FLASH beamline from that of the THz beamline is also visible. For scale, the screen's dimensions are $35\text{ mm} \times 30\text{ mm}$ while the diameter of the diamond window is 20 mm (b) shows the beamline in a partially assembled state. The positions of the mirrors within the beamline pipe are marked with blue ovals. The optical path of the alignment laser (and later the DR) is marked with dotted red arrows. The yet unassembled part of the beamline in this photo leads to the final mirror, M4, and then to the end flange where the spectrometer vessel is connected.

used for the positioning. After each mirror was added a number of functionality checks were carried out:

- Both end-switches of the stepper motors were checked for functionality. In some cases, software limits were applied on motor positions to prevent contact of the mirrors with the walls of the beamline which would cause damage.
- We checked for backlash in the motors by trying to reproduce the position of the alignment laser spot on the flange. Significant backlash was observed for both motors at mirror 1. For subsequent alignment procedures, care was taken to only drive these motors in one direction. In addition, all final aligned configurations of the beamline were checked to be reproducible after driving all motors to their end-switches.
- We checked the direction of beam deflection when a motor is driven in a particular direction. The two motors at each mirror must deflect the beam in directions within and perpendicular to the respective planes of incidence. The noted directions are used to apply a consistent sign convention on the calibration factors which are described below. These direction measurements were also integrated graphically into a redesigned user interface of the control system for the beamline (see Figure 5).

We now aim to calibrate all motors by measuring the linear calibration factor A in the equation $\Delta\theta = A \cdot S + B$ where $\Delta\theta$ is the introduced angular beam tilt or kick from a reference position and S is the motor step count. The offset B is set such that the path of the aligned laser beam positioned at all mirror centres defines zero deflection. To measure A for a particular mirror, we note the motor positions S_1 and S_2 for which the alignment laser beam is deflected to the ends of the next element in the beamline. The distances between beamline elements, s , and the projected diameter of the calibration surface, D , is known (see Figure 6). Assuming the beam is aligned and hence incident on the plane part of the converging mirror, the calibration factor is given by $A = \Theta/(S_2 - S_1)$. Here $\Theta \approx s/D$ is the angle scanned over by moving the mirror.

3.1.2 Results and Discussion

Table 2 summarises the results of the calibration. M1.1 and M1.2 are not included since these measurements were taken before realising that those motors have significant backlash error. The main source of error is the finite size of the alignment laser spot, which limits the precision any single motor measurement to about 5000 steps. Additional errors are present due to the use of the small angle approximation and also if the calibration surface is tilted by $\alpha = 45^\circ$ in the plane of calibration, as is the case for M2.1 and M3.1. However, these errors were ignored since they are of second order in the angle subtended and hence a order of magnitude small than the measurement uncertainties in this case. For example, for the calibration of motor 3.2 the measurement uncertainty causes an

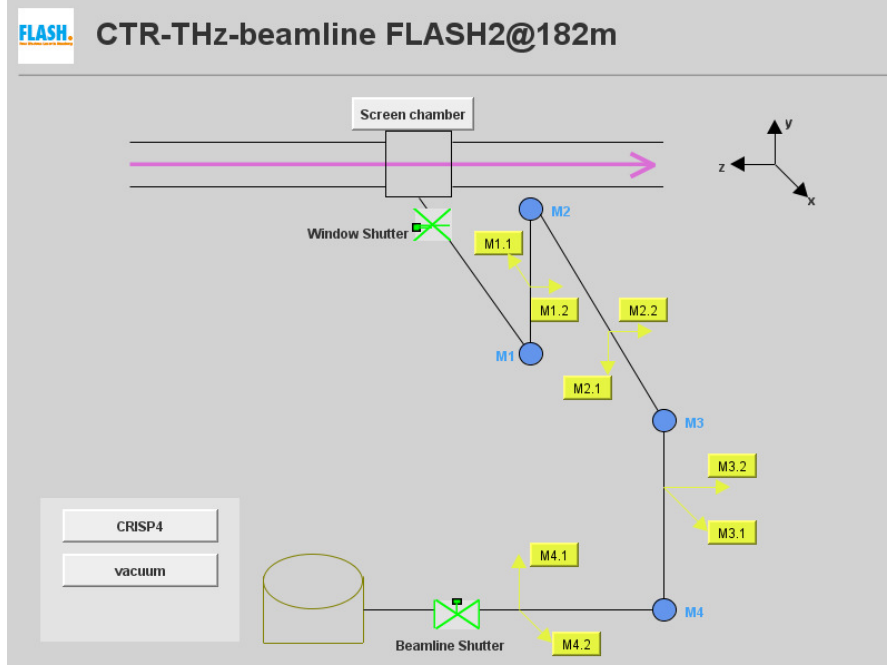


Figure 5: Remote control panel for the THz beamline. The directions that each stepper motor can be used to tilt the beam in is marked and a consistent coordinate system was implemented throughout. Each motor label is linked to the corresponding control panel where the angular deflection of the beam set. Motor step counts are mapped to angular deflections using the calibration described in the text. Additionally, the status of the vacuum shutters at the diamond window and the end of the beamline are shown. There are also buttons linked to the separate control panels for the screen chamber, spectrometer, and vacuum systems.

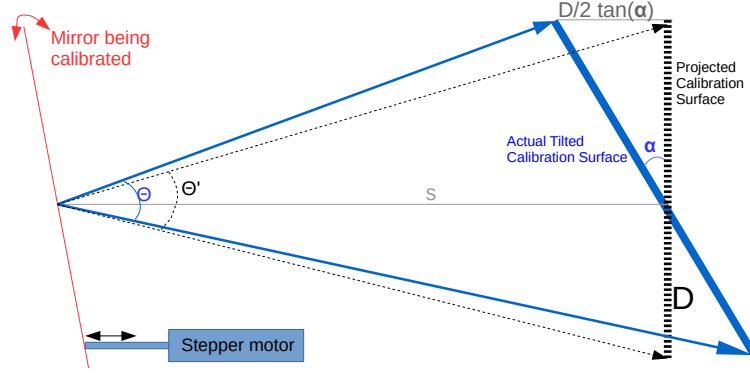


Figure 6: Calibration of mirror stepper motor by deflection of beam to the ends of a calibration surface at distance s and with projected diameter D . In certain alignment configurations the calibration surface may be tilted by an angle α which introduces additional uncertainties.

error of 3.6 % while the additional error due to the tilt of the calibration surface M4 is only 0.11 %.

Since each mirror stage is identical, we expect all motors MX.1 ($X=1,2,3,4$) to have the same calibration factor A_1 and correspondingly a second calibration factor A_2 for the other mirror tilt axis. This is indeed the case, and all measured calibration factors agree within errors. Hence, the calibration procedure was a success and the averaged calibration factors $A_1 = (5.96 \pm 0.09) \cdot 10^{-7}$ rad/step and $A_2 = (4.08 \pm 0.04) \cdot 10^{-7}$ rad/step were applied to all motors.

3.1.3 Calibration Check

When FLASH2 is in operation, the alignment laser is removed and access to the THz beamline and spectrometer is not possible. Hence to ensure that the calibration process was a success and that the response of the beam to mirror tilts can be predicted, a final check was carried out as described below.

Motor	Calibration Surface	s/mm	D/mm	$S_2 - S_1$ (steps)	$A/10^{-7}$ (rad/step)	$\Delta A/A$
M2.1	M3	392	86	$370 \cdot 10^3$	5.93	1.91%
M2.2	M3	392	86	$540 \cdot 10^3$	4.06	1.31%
M3.1	M4	1060	86	$135 \cdot 10^3$	6.01	5.24%
M3.2	M4	1060	86	$195 \cdot 10^3$	4.16	3.63%
M4.1	End flange	643.4	100	$258 \cdot 10^3$	6.02	2.74%
M4.2	End flange	643.4	100	$380 \cdot 10^3$	4.09	1.86%

Table 2: Calibration measurements for the THz beamline mirror motors using an alignment laser. The naming convention followed for the motors is MX.Y where X indicates the mirror the motor controls. $Y=1$ and $Y=2$ indicate that the motor can tilt the beam in plane of incidence and perpendicular to it respectively

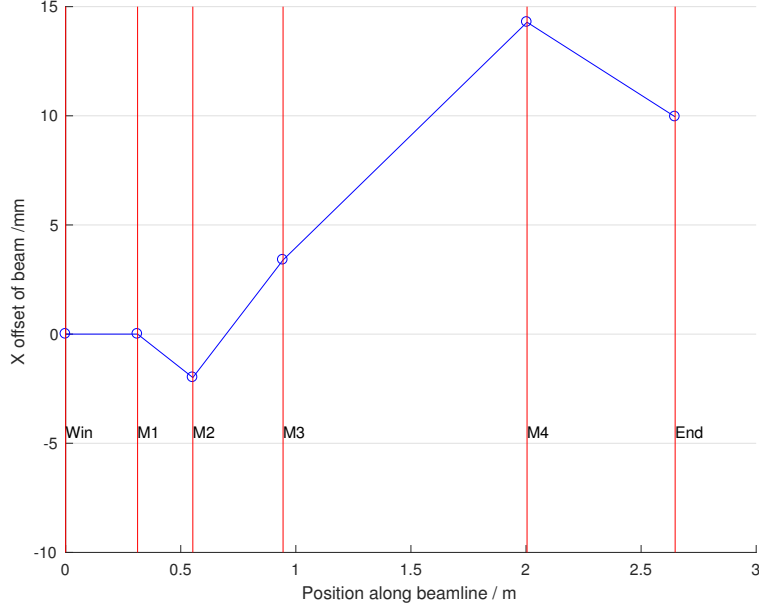


Figure 7: Linear ray optics simulation for propagation along the THz beamline. The beam is initially aligned at the window, but corrections for a hypothetical linear offset of 4.8 mm are applied at M1 and M2. This results in an intentionally misaligned beam and predicted offset of 10.0 mm at the end flange, which can be compared with measurements.

Following the formalism from Section 2.2, we have calibrated the system such that the beam is aligned when all mirror kicks $k_{Mi} = 0, i = 1 \dots 4$. Hence $x_{win} = x'_{win} = 0$ i.e. there is no linear offset or deflection at the diamond window, which is used as the reference position.

Now, we assume a hypothetical misaligned initial ray $[x_{win}, x'_{win}]$. We can realign this beam by using M_1 to tilt the beam to the central point of M_2 and then tilt M_2 to remove any remaining angular offset. Working backwards from the aligned beam $([0, 0])$ after M_2 we can solve the linear problem to calculate k_{M1}, k_{M2} giving:

$$k_1 = (1/f_1 - 1/s_2) \cdot x_{win} + (s_1(1/f_1 - 1/s_2) - 1) \cdot x'_{win}$$

$$k_2 = (x'_{win} + s_1 \cdot x'_{win})/s_2$$

where s_1 is the distance between the window and M_1 , s_2 is the distance between M_1 and M_2 , and $f_{1,2}$ are the focal lengths of the mirrors.

We then apply these corrections to our aligned beam and propagate it to predict the offset at an observation point, such as the final flange (See Figure 7). These predictions were compared with observations and found to agree, confirming that the calibration was successful.

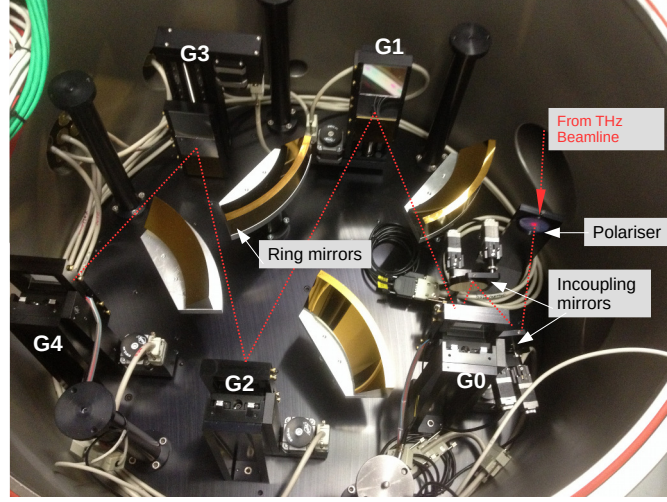


Figure 8: The spectrometer vessel. The optical path is marked with a dotted red line. The filter grating stage and the four measurement grating stages are labelled G0-G4. Full details are in the text.

3.2 THz Spectrometer

Figure 8 shows the layout of the spectrometer, which is contained in a vacuum vessel adjacent to the FLASH2 beamline. Radiation from the beamline passes through a polariser to select the component with field perpendicular to the grating grooves. The incoupling mirrors MS1 and MS2 are used for fine tuning the alignment within the vessel. Each grating stage G0-G5 (see Figure 9) can be in one of two grating positions: a far-infrared grating, and a mid infrared grating. In the third (middle) position used for alignment purposes, stages G0 and G4 have pyroelectric detectors while stages G1-3 have plane mirrors. The gratings' spacings gets progressively wider from G0 to G4. G0 acts as a low pass filter while G1-G4 disperse certain ranges of wavelengths onto their respective ring mirrors (first order diffraction peak) while specularly reflecting longer wavelengths. This arrangement suppresses higher dispersed orders at the pyro array. Each ring mirror reflects the dispersed light to an array of 30 broadband pyroelectric detectors. Hence in the far-infrared mode, the spectrum is measured in 120 channels for the wavelength range $45\text{ }\mu\text{m}$ to $435\text{ }\mu\text{m}$ while the corresponding range for the mid-infrared gratings is $5\text{ }\mu\text{m}$ to $44\text{ }\mu\text{m}$. The spectrometer is based on previous ones described in full detail in [9] and [10].

3.2.1 Functionality Checks and Alignment

- All 120 pyroelectric detector channels and the two alignment pyro detectors were individually tested by illuminating them with a triggered Nd:YAG laser pulse of wavelength 1064 nm . The shape of the trace from the ADC was verified by eye to be of the expected shape.

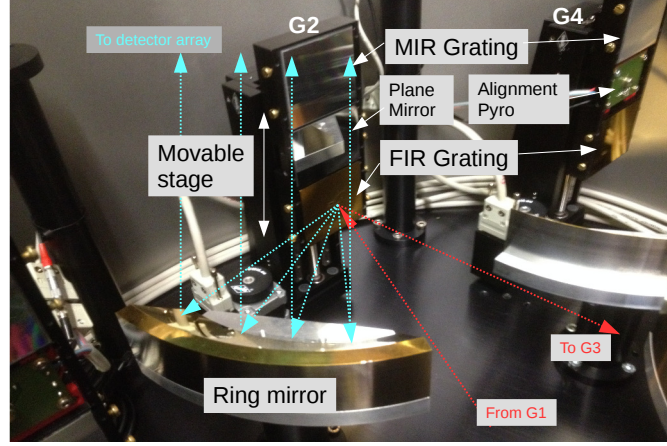


Figure 9: A closer look near grating stage G2 in the spectrometer vessel. The main optical path is marked with a dotted red line. The paths of the wavelengths dispersed at this stage are marked with dotted blue lines. The dispersed radiation is reflected by the ring mirrors to detector arrays located in a plane parallel to spectrometer floor (not yet installed in this photo). Full details are in the text.

- The polarity of the second channel of every Ethernet cable was found to be reversed versus the rest. This is due to the use of the wrong RJ45 Ethernet sockets on the pyro-boards. Nine pyro channels out of 120 were found to be non-functioning. The numbering of channels with respect to their actual array position was checked.
- The orientation of the polariser with respect to the optical axis was checked by verifying that the diffracted orders propagate in a plane parallel to the floor of the spectrometer. An optical pointer of the known beam height was used for this purpose.
- The four motors driving the incoupling mirrors were checked in a similar manner to the beamline motors. These motors were not calibrated to angular kicks, instead their extremal positions were simply set to calibrated positions of -1.0 and $+1.0$.

Incoupling Mirrors Alignment

The aim of this alignment is to centre the laser beam on the incoupling mirrors and grating stages inside the spectrometer. The alignment laser was coupled through the THz beamline and was immediately visible and well centred on the first mirror elements inside the spectrometer, indicating that the initial alignment of the THz beamline was satisfactory. Vertical alignment inside the spectrometer was checked all along the optical path using an pointer of known height. The horizontal alignment was performed iteratively by using the second mirror to centre the beam on grating stages and then using the first mirror to re-centre the beam.

4 Beam Based Commissioning

The beam-based commissioning is the second stage of the project. It begins with the final alignment of the THz beamline and spectrometer optics using actual coherent THz radiation from the screen. We then proceed to measuring and analysing the first data from the spectrometer. This stage was carried out during regular FLASH2 operation i.e. when physical access to the spectrometer area located within the tunnel is not possible. Manipulation of the mirror set-up and measurements are performed using a remote control system.

When FLASH2 operation began, a signal was immediately observed at the first alignment pyro detector indicating that the alignment procedure during technical commissioning was successful. Further fine tuning of the alignment, described below, was required to be able to observe a significant signal at the second alignment detector and ultimately at the actual measurement channels.

4.1 Measuring Intensity

All further alignment is based on intensities observed at the alignment pyros located at the filter and final stage of the spectrometer. The output from the detector is pre-amplified and then shaped into a Gaussian form before being read by an ADC at 10 MHz. For all measurements here, the shaping time was set to 1 μ s. Figure 10 shows a trace measured at the first alignment detector, which has been averaged over 100 shots to improve the signal to noise ratio.

The peak value is calculated as the average over four data points at the known bunch location. The background value is calculated as the average of all samples from the beginning of the trace to a 1000 samples before the peak. Then, the signal, which is directly proportional to the intensity at the detector, is simply the difference between the peak and background values. The error is estimated as the standard deviation in the value of the signal if calculated using each individual trace before averaging.

4.2 THz Beamline Re-Alignment

We saw signal at the first pyro but not the second, indicating a misalignment of the beam as it enters the spectrometer. To realign the beam, the methods tried were as follows:

- Assume an initial linear offset in the y-direction at the diamond window. Apply corrections to M1 and M2 for this offset as described in Section 3.1.3. Scan over different offsets and measure the intensity at the first pyro for each to find the maxima. Check if a signal is seen at the second pyro for this correction setting.
- Assume a certain angular tilt, θ_s , of the diffraction radiation screen. This causes a corresponding linear offset $\theta_s \cdot r_{S \rightarrow W}$, and an angular offset $\theta_w = \theta_s$ at the diamond window. Here $r_{S \rightarrow W}$ is the known distance between the diffraction screen and the window. As above, correct for these while scanning over θ_s to find a maximum in intensity.

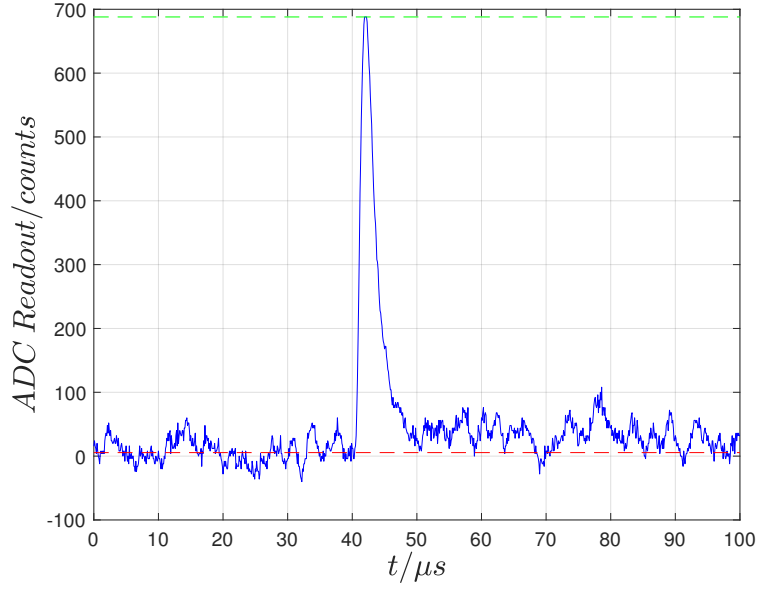


Figure 10: A typical trace measured at a pyroelectric detector, averaged over 100 shots to improve the signal to noise ratio. The signal is calculated as the difference between average value of four peak points (green) and the average background value before the radiation arrives (red).

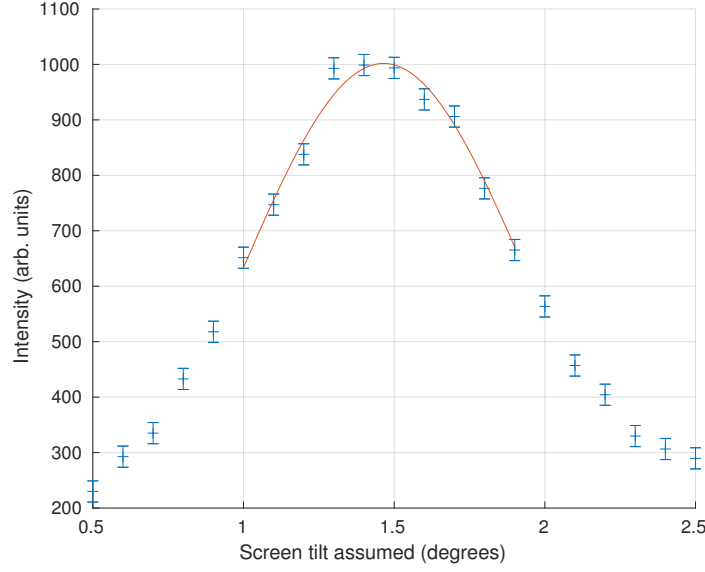


Figure 11: A scan of intensity at the first pyro versus assumed tilt of the radiation screen for which mirror corrections are applied. A Gaussian peak is fit to find the peak value of $1.4 \pm 0.1^\circ$.

Results and Discussion

The first method from above did give an intensity maximum at the first pyro, but no signal was observed at the final pyro. The scan using the second method, shown in Figure 11, cause in increase in intensity by a factor of about 10 at the peak value of $\theta_s = 1.4 \pm 0.1^\circ$. The precision is limited by the resolution of the screen tilt scan. This scan was successful since a signal was also observed at the second alignment pyro when the calculated correction was applied. Similar radiation screens at other instruments were measured to have orientation errors of the same order as θ_s . Hence this is a reasonable correction to apply, and we can proceed to the final beam based alignment using incoupling mirrors.

4.3 Internal Spectrometer Alignment

The aim of this final alignment is to centre the profile of the diffraction radiation at both alignment pyros. Since the polariser selects only the horizontal component of radiation entering the spectrometer the expected radiation profile has a central maximum when projected in the Y direction (See Figure 12). In the X direction, the radiation profile has two maxima and a central minimum. The alignment procedure can be applied independently in the X and Y directions and is as follows:

1. Using the first incoupling mirror (MS1) as the scanning device, measure the intensity profiles at the first and second alignment pyros.

2. Fit peaks (one for Y or two for X) to the measured intensity profiles to find the positions of MS1 for which the intensity profile is centred on each detector.
3. Using a similar linear optics method as described in Section 3.1.3, and the known distances between the elements in the set-up, we can calculate new positions for both incoupling mirrors.
4. Iterate this procedure till the newly found positions converge and the profile is centred on both detectors.

Results and Discussion

Figure 13 shows a single iteration of the scans in both directions and at both detectors. Two iterations of the procedure, plus a final check for centring were required before alignment was achieved. This alignment procedure was successful since we were able to measure signal at the detector channels after it was complete.

The first pyro is only 175 mm away from scanning mirror while the second pyro is at 1.64 m. Hence we expect the radiation profile to be ‘narrower’ at the second detector by about a factor of 10, which is apparent from the data. The Gaussian fits are simply a reproducible method to find the centre of the profile, not analytic descriptions of the profile. This explains the poor fit in some regions. This is not an issue since the single or double peak structure itself is clearly visible in the raw data and the visible location of the centre agrees with the fits.

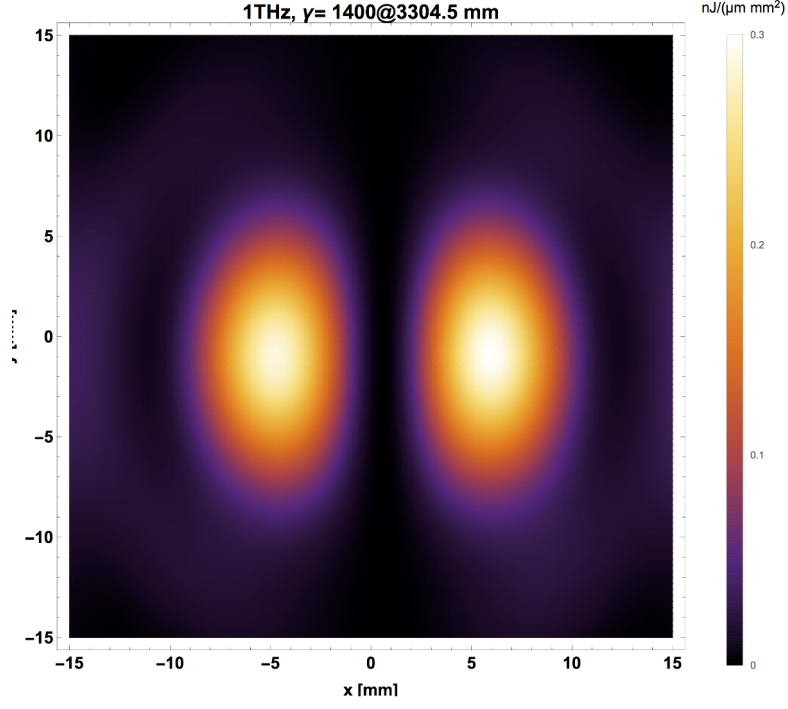


Figure 12: Simulated intensity distribution of coherent diffraction radiation at the first alignment pyro inside the spectrometer. A double lobe profile is seen since the polariser has chosen the horizontal field component (at the spectrometer) only. Hence, when scanning over this profile by moving the incoupling mirrors x - and y -directions, we expect to see a double peak structure and single peak structure respectively. Simulations performed using THzTransport [8].

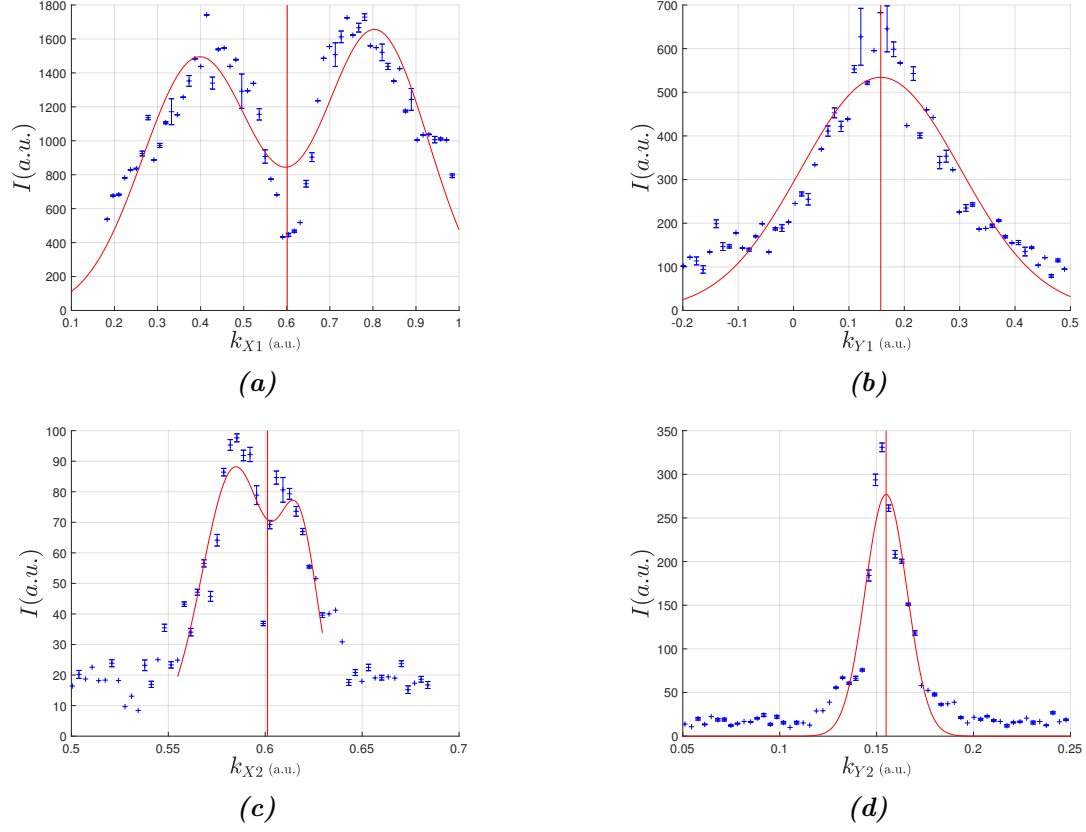


Figure 13: Intensity scans over the diffraction radiation profile at the alignment detectors in the spectrometer vessel for alignment of the incoupling mirrors. Scans were performed at the first (top row) and second (bottom row) alignment pyros in the horizontal (left column) and vertical (right column) directions respectively. The vertical red lines mark the fitted centres of the Gaussian and double Gaussian intensity distributions.

5 First Measurements of Spectra

5.1 Methods

We now try to perform the first actual measurements using the spectrometer. The gratings were set to long wavelength and short wavelength modes in turn, and the signal was measured in 120 channels as described in Section 4.1. The signals from channels which are known to be dead, or have reversed polarity as determined by the functionality checks (see Section 3.2.1) are ignored or negated respectively.

DR spectra have a characteristic sharp fall in intensity at short wavelengths. Initial simulations suggest that this occurs at about $40\text{ }\mu\text{m}$ for our set-up. To ensure sufficient intensity at short wavelengths, which allows us to check that all gratings and detectors are functioning, we moved the diffraction radiator directly into the path of the electron beam for certain measurements. This effectively allows us to see a TR spectrum, which has no intrinsic short wavelength cut-off in the measured wavelength range.

To compress electron bunches at FLASH, a longitudinal energy chirp is applied to them. Then, they pass through a magnetic chicane (compressor) where their trajectory length depends on energy. Hence compression is achieved by, for example, allowing high-energy electrons in the rear of the bunch to catch up with the low energy head. The magnitude of the energy chirp (and hence the compression) can be varied by changing the relative phase of the accelerating electric field in adjacent RF cavities. One such phase setting, ACC23, was varied in the range $\phi = -2^\circ$ to 1° for spectra measurements. By convention, higher phase settings increase the bunch compression. Gaussian bunch shapes were then fitted to the measured form factors, which allows us to qualitatively determine if the spectrometer is sensitive to changing bunch lengths as expected. As Figure 3 shows, the form factor for a Gaussian bunch with RMS length σ_z is:

$$|F_{gauss}(\lambda)| = \exp[-2(\pi\sigma_z/\lambda)^2]. \quad (3)$$

Determining the spectrum from the measured signals from ADC channels requires the spectral response function of the set-up. Detailed simulations by Stephan Wesch for a previous spectrometer were adapted for this new set-up to calculate the response[9]. These simulations are based on the THzTransport package [8] and account for production of the coherent radiation, transport through the beamline and spectrometer, diffraction at the gratings, spectral response of the detectors, etc. The calculated responses, $R(\lambda_i), i = 1...240$ (in units of $ADC\ counts/nC^2$) for each channel can then be used to find the absolute form factor, $|F|$, via the relation:

$$|F| = \sqrt{\frac{S(\lambda_i)}{R(\lambda_i) \cdot Q^2}} \quad (4)$$

where $S(\lambda_i)$ is the signal (in ADC counts) at a particular channel and Q is the total charge of the electron bunch.

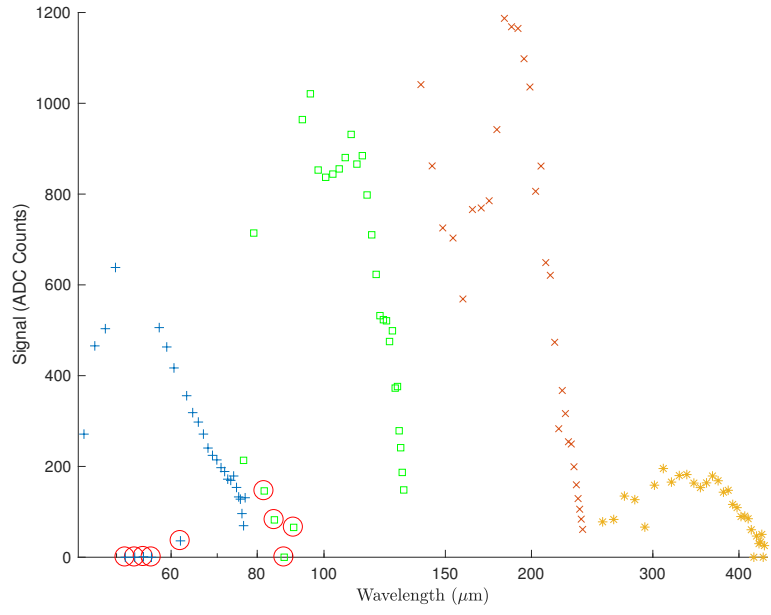


Figure 14: Uncalibrated signal measurements from the spectrometer in long wavelength mode ($45\mu\text{m}$ to $435\mu\text{m}$). These data were taken with the DR screen in the centred position and the compression setting $\phi = 0$. Non-functioning pyro channels are circled in red.

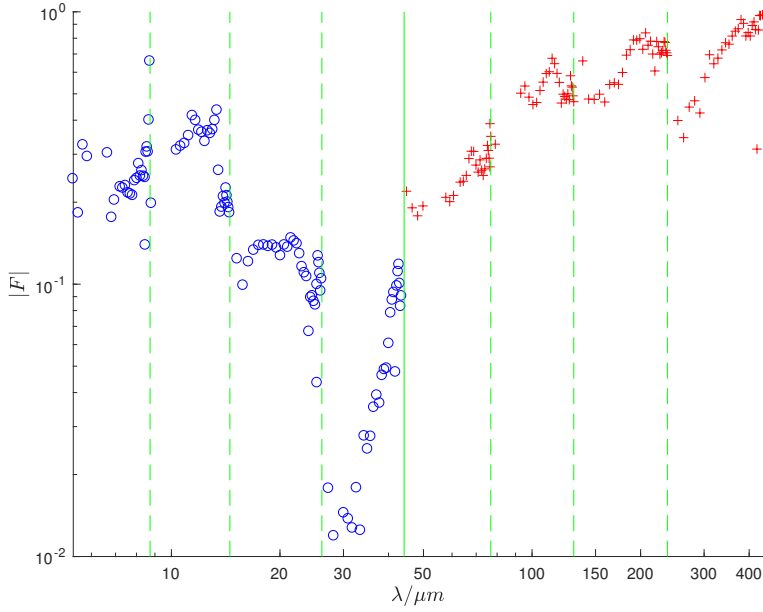


Figure 15: A full measured TR spectrum. These data were taken with the DR screen positioned such that the electron beam strikes it directly. The compression setting was $\phi = +1^\circ$. Due to an additional linear gain factor in the detector electronics not accounted for in the response simulations, we normalise the form factor to 1 at long wavelengths using the average value of the 5 longest wavelengths. MIR mode data (blue) is separated from FIR data (red) by a solid green line. Measurements from different grating stages are demarcated with dashed lines. Both axes are scaled logarithmically.

5.2 Results and Discussion

Figure 14 shows the signals measured at all long wavelength channels. The nine broken channels have been circled in red. These are excluded from all further analysis. The reversed polarity of some channels has been accounted for, hence all signals are positive. Signal is seen at all grating stages, indicating that the alignment procedure and functionality checks were successful. There are large discontinuities between data from adjacent stages. Since the bunch profile and hence the form factor must be continuous, we expect that the large steps will disappear once the response function is applied. In this centred screen position, no signal is seen in short wavelength mode. This is likely due to the characteristic DR spectrum cut-off mentioned above.

In order to be able to see signal at short wavelengths too, the screen was moved vertically so that the electron beam strikes it directly. The compression was also increase by setting $\phi = 1^\circ$. Figure 15 shows a full spectrum measured with these settings. The form factor has been computed using the simulated response. Signal is seen at all stages in both

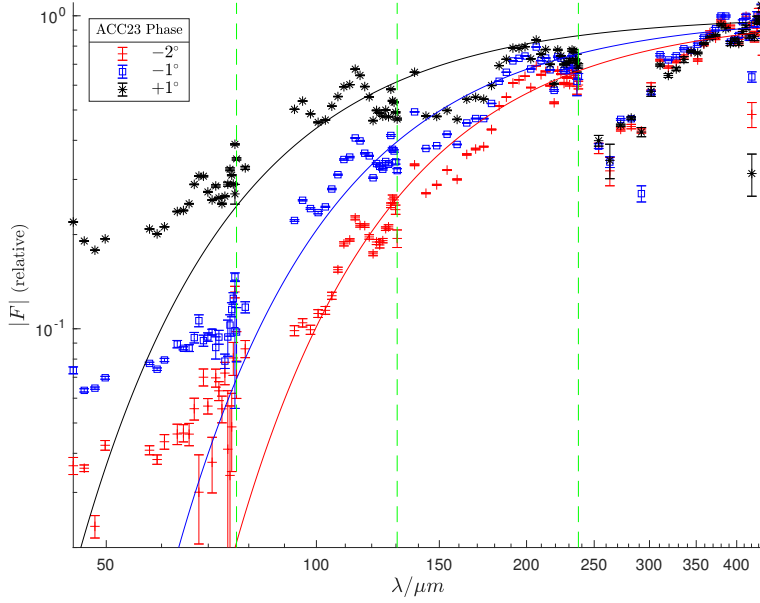


Figure 16: Measured spectra for different compression settings and fits for a Gaussian bunch shape. Due to possible issues with misalignment at the final grating stage, only the 5 final points from this set were used for the fit. Measurements from different grating stages are demarcated with dashed green lines. Both axes are scaled logarithmically.

modes, indicating that all gratings are in working order. The response successfully removes most discontinuities, however there are still large steps between measurements from the G3 and G4 grating stages in both short and long wavelength data. This could be due to incorrectly oriented gratings on the final stage. Since the gratings are blazed to direct most intensity to the first order diffraction peak, a 180° rotation would cause a significant change in the response. The large steps could also be caused by misalignment of the ring mirrors with respect to the detector, again significantly affecting the response. There is also an oscillatory structure in the G2 data for both wavelength modes. This feature is persistent when the compression settings are changed, indicating that it is not a bunch feature, but rather a problem with the response simulations. These errors must be checked further using simulations and then corrected if necessary after re-opening the spectrometer vessel.

Figure 15 shows measured spectra for different compression settings and fits for a Gaussian bunch shape. Figure 15 lists the fitted bunch lengths. Errors for individual points in the spectra were estimated from averaged ADC traces. The errors in the mean background and peak values were combined to find the uncertainty. It would be more accurate to analyse errors in each ADC trace individually and combine these, but this was not possible since only averaged traces were saved for offline analysis. The errors in

ACC23 Phase (ϕ)	$\sigma_z/\mu m$
-2°	34 ± 1.0
-1°	28.3 ± 0.8
$+1^\circ$	20.5 ± 1.0

Table 3: Fitted RMS bunch lengths for different compression settings. A Gaussian bunch shape was assumed for these fits. The errors are from the confidence intervals in the fitting program.

bunch lengths are simply the confidence intervals from the fitting program. These are likely underestimated since the fit is poor and many systematic deviations from it are apparent. This is because the model is crude, and could be improved by adding more parameters eg. a super-Gaussian profile. However, it is clear that the bunch lengths decrease with increasing compression, and the lengths are of the same order as expected at FLASH2. Hence the spectrometer is successful as a diagnostic instrument in this preliminary test.

6 Conclusions

The technical and beam based commissioning of the spectrometer was completed. Functionality checks were carried out on the components of the THz beamline and spectrometer and most issues were fixed. It remains possible that the surface of some gratings is damaged and possibly misoriented. The mirrors of the THz beamline were calibrated for absolute angular kick applied to a beam along both tilt axes. Initial alignment of the THz beamline and spectrometer was performed using an optical laser. During beam based commissioning, the THz beamline was aligned by correcting for a tilt of the radiation screen. The final alignment of the spectrometer was performed iteratively by centring the coherent diffraction radiation profile on both alignment pyroelectric detectors. Intensity was detected at all functioning measurement channels. It was possible to measure full calibrated spectra which change as expected when the bunch length is varied. These measurements strongly indicate that the alignment and functionality checks carried out were successful. For full spectra measurements and reconstruction, further work is needed which could not be completed due to time constraints. The diffraction radiator will be replaced with an off axis transition radiation screen and a kicker magnet set-up allowing TR generation during user runs. Further checks of the gratings are required to ensure that they are oriented correctly, and the alignment of the pyro arrays must also be checked. Broken detectors must be fixed, and a careful re-evaluation of the response function for all channels is required. The completion of these steps will make it possible to reconstruct bunch profiles and use the spectrometer as a diagnostic tool for precision bunch compression control during regular operation of FLASH2.

References

- [1] S. Ackermann et al. Simultaneous Operation of a Multi Beamline FEL Facility. In *International Free-Electron Laser Conference*, pages 301–304, Nara, Japan, 2012.
- [2] W. Ackermann et al. Operation of a free-electron laser from the extreme ultraviolet to the water window. *Nature Photonics*, 1:336, 02 2007.
- [3] O. Altenmueller, R. Larsen, and G. Loew. Investigations of TravelingWave Separators for the Stanford TwoMile Linear Accelerator. *Review of Scientific Instruments*, 35(4):438–442, April 1964.
- [4] S. Casalbuoni et al. Ultrabroadband terahertz source and beamline based on coherent transition radiation. *Physical Review Special Topics - Accelerators and Beams*, 12(3):030705, 2009.
- [5] O. Grimm and P. Schmser. Principles of longitudinal beam diagnostics with coherent radiation. Technical Report TESLA FEL 2006-03, April 2006.
- [6] E. Hass et al. Longitudinal bunch profile reconstruction using broadband coherent radiation at FLASH. In *International Beam Instrumentation Conference*, Oxford, 2013.
- [7] M. Rhys et al. Time-resolved electron beam phase space tomography at a soft x-ray free-electron laser. *Physical Review Special Topics - Accelerators and Beams*, 12(5):050704, May 2009.
- [8] B. Schmidt. Thz transport code. Personal communication.
- [9] S. Wesch. *Echtzeitbestimmung longitudinaler Elektronenstrahlparameter mittels absoluter Intensitäts- und Spektralmessung einzelner kohärenter THz Strahlungspulse*. PhD thesis, Universität Hamburg, Diss. DESY-THESIS-2012-052, 2012.
- [10] S. Wesch et al. A multi-channel THz and infrared spectrometer for femtosecond electron bunch diagnostics by single-shot spectroscopy of coherent radiation. *Nuclear Instruments and Methods in Physics Research Section A: Accelerators, Spectrometers, Detectors and Associated Equipment*, 665: 40–47, February 2011.
- [11] S. Wunderlich et al. *Development and Commissioning of a Double-Prism Spectrometer for the Diagnosis of Femtosecond Electron Bunches*. PhD thesis, Verlag Deutsches Elektronen-Synchrotron DESY-THESIS-2016-038, 2016.